Journal of Inorganic Biochemistry 105 (2011) 52–57

Contents lists available at ScienceDirect

Journal of Inorganic Biochemistry

journal homepage: www.elsevier.com/locate/jinorgbio

Ca^{2+}-induced self-assembly in designed peptides with optimally spaced *gamma*-carboxyglutamic acid residues

Qiuyun Dai [a,*], Mingxin Dong [a], Zhuguo Liu [a], Mary Prorok [b,c], Francis J. Castellino [b,c,*]

[a] Institute of Biotechnology, Beijing 100071, China
[b] Department of Chemistry and Biochemistry, University of Notre Dame, IN 46556, USA
[c] W.M. Keck Center for Transgene Research, University of Notre Dame, IN 46556, USA

ARTICLE INFO

Article history:
Received 5 April 2010
Received in revised form 8 August 2010
Accepted 1 October 2010
Available online 8 October 2010

Keywords:
gamma-carboxyglutamic acid
Helix–helix interactions
Peptide self-assembly

ABSTRACT

We have previously elucidated a new paradigm for the metal ion-induced helix–helix assembly in the natural γ-carboxyglutamic acid (Gla)-containing class of conantokin (con) peptides, typified by con-G and a variant of con-T, con-T[K7Gla], independent of the hydrophobic effect. In these "metallo-zipper" structures, Gla residues spaced at i, i + 4, i + 7, i + 11 intervals, which is similar to the arrangement of *a* and *d* residues in typical heptads of coiled-coils, coordinate with Ca^{2+} and form specific antiparallel helical dimers. In order to evaluate the common role of Gla residues in peptide self-assembly, we extend herein the same Gla arrangement to designed peptides: NH_2–(γLSγEAK)$_3$–$CONH_2$ (peptide 1) and NH_2–γLSγEAKγLSγQANγLSγKAE–$CONH_2$ (peptide 2). Peptide 1 and peptide 2 exhibit no helicity alone, but undergo structural transitions to helical conformations in the presence of a variety of divalent cations. Sedimentation equilibrium ultracentrifugation analyses showed that peptide 1 and peptide 2 form helical dimers in the presence of Ca^{2+}, but not Mg^{2+}. Folding and thiol-disulfide rearrangement assays with Cys-containing peptide variants indicated that the helical dimers are mixtures of antiparallel and parallel dimers, which is different from the strict antiparallel strand orientations of con-G and con-T[K7γGla] dimers. These findings suggest that the Gla arrangement, i, i + 4, i + 7, i + 11, i + 14, plays a key role in helix formation, without a strict adherence to strand orientation of the helical dimer.

1. Introduction

Helix–helix interactions, such as those that occur in two-stranded or multiple stranded coiled-coil domains [1–3], four helix bundles [4], membrane-spanning helical bundles [5], or EF hands [6], are important to the structural organization and function of numerous proteins. In several natural proteins and model peptide systems, metal ions can aid in the formation of coiled-coils and helical bundles through the stabilization of preexisting folded components into superstructures [7–9], and/or by directing the folding and subsequent assembly of polypeptide chains [10–13]. In both categories, cooperative metal ion coordination among subunits initiates oligomerization, and/or guides relative chain orientation, while hydrophobic interactions at the interchain interface remain the predominate forces that drive and stabilize complex formation.

Recently, we found a new mechanism for coiled-coil formation in natural γ-carboxyglutamic acid (Gla)-containing peptides, showing that interhelical calcium ion coordination directly controls the formation of α-helical coiled-coils with a high specificity of chain orientation. These principles were established in studies with the natural conantokin peptide, con-G, and a variant of another such peptide, con-T[K7Gla] [14–16]. These peptides contain an i, i + 4, i + 7, i + 11 arrangement of Gla residues. This coiled-coil superstructure is unusual in the realm of helix–helix interactions, because the bulk of the binding energy associated with subunit association appears to derive from interhelical Gla–Ca^{2+} coordination, rather than hydrophobic interactions. In order to affirm and generalize the common role of Gla residues in self-assembly, we extend studies herein to two designed peptides NH_2–(γLSγEAK)$_3$–$CONH_2$ (peptide 1) and NH_2–γLSγEAKγLSγQANγLSγKAE–$CONH_2$ (peptide 2), which were mainly derived from the modification of the two helical peptides ((LEALEGK)$_5$ and (LAELKGE)$_5$) that dimerize in parallel and antiparallel orientations, respectively [17]. In these designed peptides, the heptad repeats were shortened to three repeats, and hydrophobic L residues at *a* or *d* positions spaced at i, i + 4, i + 7, i + 14, were replaced by Gla residues; other residues, such as E, A and G, were made to maintain a balance between peptide hydrophobicity and hydrophilicity. The results showed that peptide 1 and peptide 2 form helical dimers in the presence of Ca^{2+}, but not Mg^{2+}, though they alone exhibit no helical conformation. Folding and thiol-disulfide rearrangement assays with Cys-containing peptide 1 variants indicated that the helical dimers were mixtures of antiparallel and parallel dimers.

* Corresponding authors. Dai is to be contacted at the Institute of Biotechnology, Beijing 100071, China. Tel.: +86 10 66948897; fax: +86 10 63833521. Castellino, W.M. Keck Center for Transgene Research, University of Notre Dame, IN 46556, USA. Tel.: +1 574 6319120; fax: +1 574 6314048.
E-mail addresses: qy_dai@yahoo.com (Q. Dai), fcastell@nd.edu (F.J. Castellino).

0162-0134/$ – see front matter © 2010 Elsevier Inc. All rights reserved.
doi:10.1016/j.jinorgbio.2010.10.002

2. Results

2.1. Ca^{2+}-induced helix formation and helix–helix assembly in designed peptides with optimally spaced Gla residues

Two simple hydrophilic peptides with a Gla arrangement of i, i + 4, i + 7, i + 11, i + 14, synthesized for this study, as well as their α-helical heptad repeat assignments (*a*–*g*), are shown in Fig. 1. In peptide 1 and peptide 2, Gla residues were arranged in the *a* and *d* positions, similar to con-G, con-T[K7Gla], and the hydrophobic residue arrangement at *a* and *d* positions of heptad repeats in coiled-coils. Glu and Lys occupied the *e* and *g* positions, which are anticipated to produce ionic interactions at the interhelical face. Circular dichroism (CD) (Fig. 2) and analytical sedimentation equilibrium ultracentrifuge (AEC, Fig. 3) results for designed peptides, in the absence or presence of metal ions, are summarized in Table 1. In the absence of metal ions, peptide 1 and peptide 2 failed to form α-helices. However, the addition of 20 mM Ca^{2+}, pH 6.5, resulted in 51% and 22% of α-helix for peptide 1 and peptide 2, respectively. In the apo form, peptide 1 and peptide 2 exhibited a monomeric MW_{app} of 3330 and 3470, which are within 20% of their calculated sequence-based MW. In the presence of 20 mM Ca^{2+}, this value is increased to 5480 and 5910, respectively. When taking a bound Ca^{2+} stoichiometry of 9 into account (*vide supra*), the MW_{app} of both Ca^{2+}-associated peptides is consistent with a fractional dimer content of 0.58 and 0.67, respectively. The corresponding dimer association constants for peptide 1 and peptide 2 are $1.1 \times 10^4\ M^{-1}$ and $2.1 \times 10^4\ M^{-1}$. Similarly, Sr^{2+} and Ba^{2+} also induced significant dimer formation in these peptides. In contrast to Ca^{2+}, Sr^{2+} and Ba^{2+}, neither Mg^{2+}, Zn^{2+} nor Mn^{2+} induced measurable self-association of the two designed peptides, despite the higher content of α-helix in these metal ion/peptide complexes compared to Ca^{2+}-bound peptides (Table 1). Hence, metal ions involved in relatively weak intrahelical binding appear to be more conducive to intermolecular strand association than tighter-binding metal ions.

These proposed binding modes are further established by measurements of the stoichiometries of Ca^{2+} binding to the designed peptides using isothermal titration calorimetry (ITC; Fig. 4). Despite the small enthalpies that accompany incremental additions of $CaCl_2$ into peptides 1 and 2, large differences in the molar ratios of Ca^{2+} to peptide are evident following deconvolution of the heat changes. The heat changes showed two distinct classes of binding sites for peptide 1 ($n_1 = 1.0$, $n_2 = 6.3$) and peptide 2 ($n_1 = 3.0$, $n_2 = 5.6$) in the presence of Ca^{2+} (Fig. 4a–b), but a type of binding site in the presence of Mg^{2+} (n = 2–3, Fig. 4c–d). The K_d value for Ca^{2+} binding to first class of site of peptide 1 was not calculated because of smaller heat changes, the K_d value obtained for second class of site was 68 μM, whereas Mg^{2+} displayed a K_d value of 150 μM (n = 1.9). Similar results were obtained for Ca^{2+} binding to peptide 2. Its K_d values for the first and second classes of sites were 135 μM and 180 μM, respectively. These results indicate that the binding modes of Ca^{2+} to these peptides are different from that of Mg^{2+},

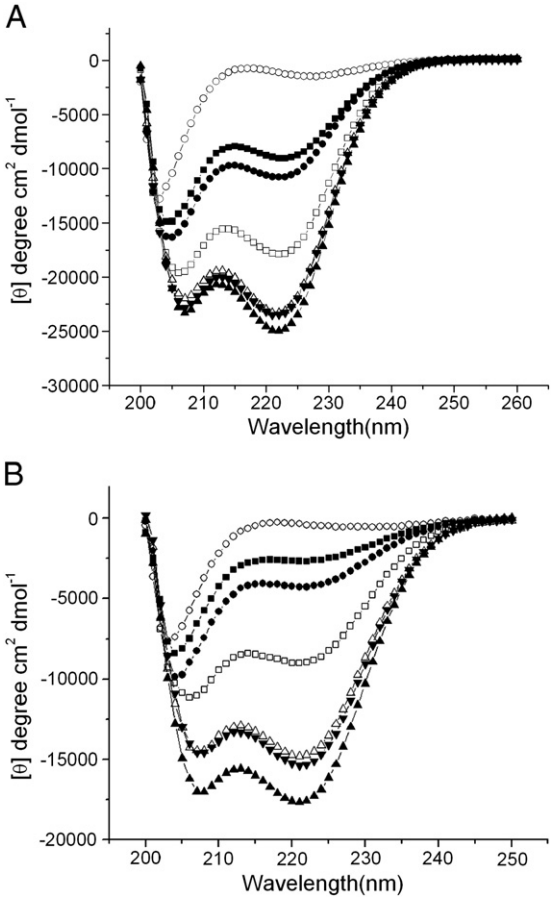

Fig. 2. CD spectra of peptide 1 and peptide 2 in the presence and absence of metal ions. Spectra were recorded at 25 °C in 10 mM sodium borate/100 mM NaCl, pH6.5. Peptide concentrations were 35 μM. The metal ion concentrations were 20 mM for Ca^{2+}, Mg^{2+}, Sr^{2+} and Ba^{2+} and 5 mM for Zn^{2+} and Mn^{2+}. (○) Buffer; (□) Ca^{2+}; (△) Mg^{2+}; (●) Sr^{2+}; (■) Ba^{2+}; (▲) Zn^{2+}; (▼) Mn^{2+}.

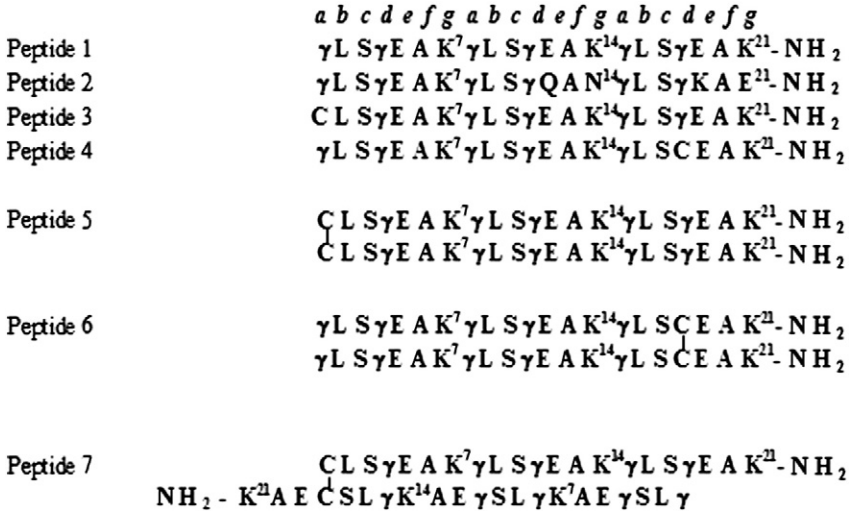

Fig. 1. Primary sequences of the designed peptides. The heptad repeat for each peptide is denoted a–g and a'–g' (for antiparallel strands).

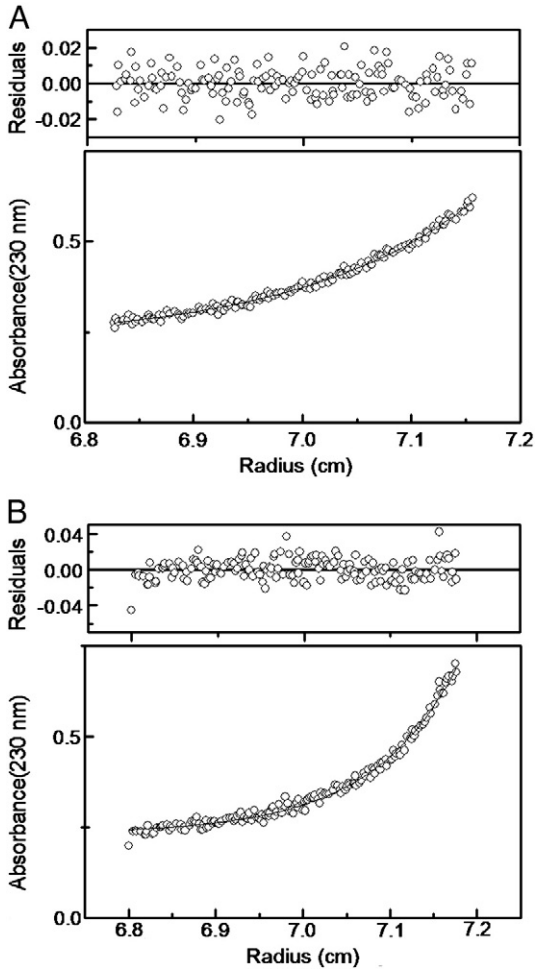

Fig. 3. Sedimentation equilibrium results for peptide 1 at 20 °C and in 10 mM sodium borate/100 mM NaCl, pH6.5 in the absence and presence of 10 mM $CaCl_2$. The concentration of peptide was 150 μM. The data were collected at a rotor speed of 45,000 rpm. (a) Peptide 1; (b) peptide 1 + 10 mM Ca^{2+}. The MW_{app} values corresponding to the fitted data were 3140 for (A) and 5180 for (B).

Ca^{2+} binding to peptides 1 and 2 is involved in monomeric helical conformational changes and helix–helix interactions.

2.2. Helical strand orientation in peptide 1

Peptide 1 was selected to ascertain the relative strand alignment of the putative dimer, i.e., parallel or antiparallel, since it had a high content of the helical dimer. To examine its strand orientation, two Cys-containing peptide (peptide 3 and peptide 4) variants were designed. Peptide 3 and peptide 4 contain a Cys substitution at the N-terminus (Gla^1C) and at the C-terminal region ($Gla^{18}C$). Because our initial model of the peptide helical dimer consisted of a Gla core (designated as positions *a* and *d* in the heptad template), involving Gla residues 1, 4, 8, 11, 15, and 18, the placement of Cys in each variant also occurs at positions *a* or *d* in the heptad repeat (Fig. 1). Peptides 5, 6 and 7, the parallel homodimer and antiparallel disulfide-linked heterodimer of Cys-containing peptides 3 and 4, were also synthesized as controls for the characterization of the strand orientation of peptide 1 in the folding and equilibrium experiments. Using the two Cys-containing variants, the preference for relative helix orientation of peptide 1/Ca^{2+} was assessed by examining relative amounts of oxidized product as previously described [14,18–20]. The distribution of products resulting from the co-incubation of peptide 3 and peptide 4 in the absence and presence of various metal ions is shown in the series of chromatograms in Fig. 5. With Ca^{2+} present, the amount of the disulfide-linked heterodimeric peptide 7 was not predominant and was different from the folding of Cys-containing con-G [14], in which the heterodimer is almost one folding product. These results suggest that the orientation of peptide 1/Ca^{2+} is mixture of antiparallel and parallel strands.

This helical orientation was also supported by the results of exchange experiments in which the N- and C-terminal disulfide-linked homodimers 5 and 6 were individually incubated with Cys-containing peptide 4 and 3, respectively. Beginning with peptide 4 and peptide 5 in a 2:1 molar ratio in the presence of Ca^{2+}, homodimer 5 exchanged rapidly with peptide 4, and the products were disulfide-linked heterodimeric peptide 7 and the remaining homodimeric peptide 5 (Fig. 6). The same results were observed with equilibrium experiments employing peptide 3 and peptide 6. These results reinforce the conclusion that in the presence of Ca^{2+}, peptide 1 can self-associate in both parallel and antiparallel motifs.

Table 1
Metal ion effects on the secondary structure and MW_{app} of the designed peptides.

Peptide	Metal ion[a]	% Helix[b]	MW_{app}[c]	f_{di}[d]	n[e]	K_d[e](μM)
Peptide 1	None	0	3330	0	0	0
	Ca^{2+}	51	5480	0.58	2.0[f];12.6[f]	n.d.;68
	Mg^{2+}	69	3170	0	1.9	318
	Zn^{2+}	70	4190	0.19	n.d.	n.d.
	Mn^{2+}	75	3330	0	n.d	n.d.
	Ba^{2+}	22	5350	0.43	n.d..	n.d.
	Sr^{2+}	28	6080	0.69	n.d.	n.d.
Peptide 2	None	0	3470	0	0	0
	Ca^{2+}	22	5910	0.67	6.1[f];11.2[f]	135;180
	Mg^{2+}	41	3570	0	3.2	150
	Zn^{2+}	43	3850	0.05	n.d.	n.d.
	Mn^{2+}	50	4150	0.14	n.d.	n.d.
	Ba^{2+}	1	5200	0.34	n.d.	n.d.
	Sr^{2+}	6	4870	0.30	n.d.	n.d.
Peptide 5	None	0	5400	0	0	0
	Ca^{2+}	29	7890	0.48	n.d.	n.d.
	Mg^{2+}	36	5860	0.12	n.d.	n.d
	Mn^{2+}	40	n.d.	n.d.	n.d.	n.d.
	Ba^{2+}	20	10270	0.80	n.d.	n.d.
	Sr^{2+}	20	9480	0.72	n.d.	n.d.

[a] For CD experiments, the metal ion concentrations were 20 mM for Ca^{2+}, Mg^{2+}, Sr^{2+} and Ba^{2+} and 5 mM for Zn^{2+} and Mn^{2+}. For AEC experiments, the metal ion concentrations were 10 mM for Ca^{2+}, Mg^{2+}, Sr^{2+} and Ba^{2+} and 5 mM for Zn^{2+} and Mn^{2+}. The buffer was 10 mM $NaBO_3$/100 mM NaCl, pH 6.5. In all instances, the Cl^- salts of the metals were used.

[b] The percentage of α-helix was estimated from CD measurements. The concentrations of peptide 1 and 2 were 35 μM, while the concentrations of disulfide-containing peptides were 17.5 μM.

[c] Values for MW_{app} represent the average of 2–4 separate analyses (3 scans per analyses). The variability, in all cases, was ≤8%.

[d] Fractional dimer (f_{di}) content was calculated as described previously [14].

[e] Values for n (stoichiometry of metal ion binding) and K_d were determined by ITC as indicated in "Experimental procedures".

[f] Values was calculated from the ratios of [Ca^{2+}]/[peptide 1 monomer] or [peptide 2 monomer], n values for dimers should be the half of these values.

3. Discussion

Design of proteins and peptides in specific conformations provides opportunities to engineer specific properties, e.g., catalysis, receptor binding, membrane and blood barrier permeability, into small molecules that could serve as readily manipulatable new drugs. To be successful in such design strategies, an understanding of the forces that allow proteins to fold into specific stable tertiary structure must be better understood. Multimeric ensembles of helices, such as coiled-coils and helical bundles, have received a great deal of attention in this regard, and allow specific folding of proteins using very small regions of the protein of interest, and/or oligomerization of proteins and peptides into multisubunit structures.

We have previously found that the Ca^{2+}-assisted self-association of con-G and con-T[K7Gla] is contingent upon an i, i + 4, i + 7, i + 11

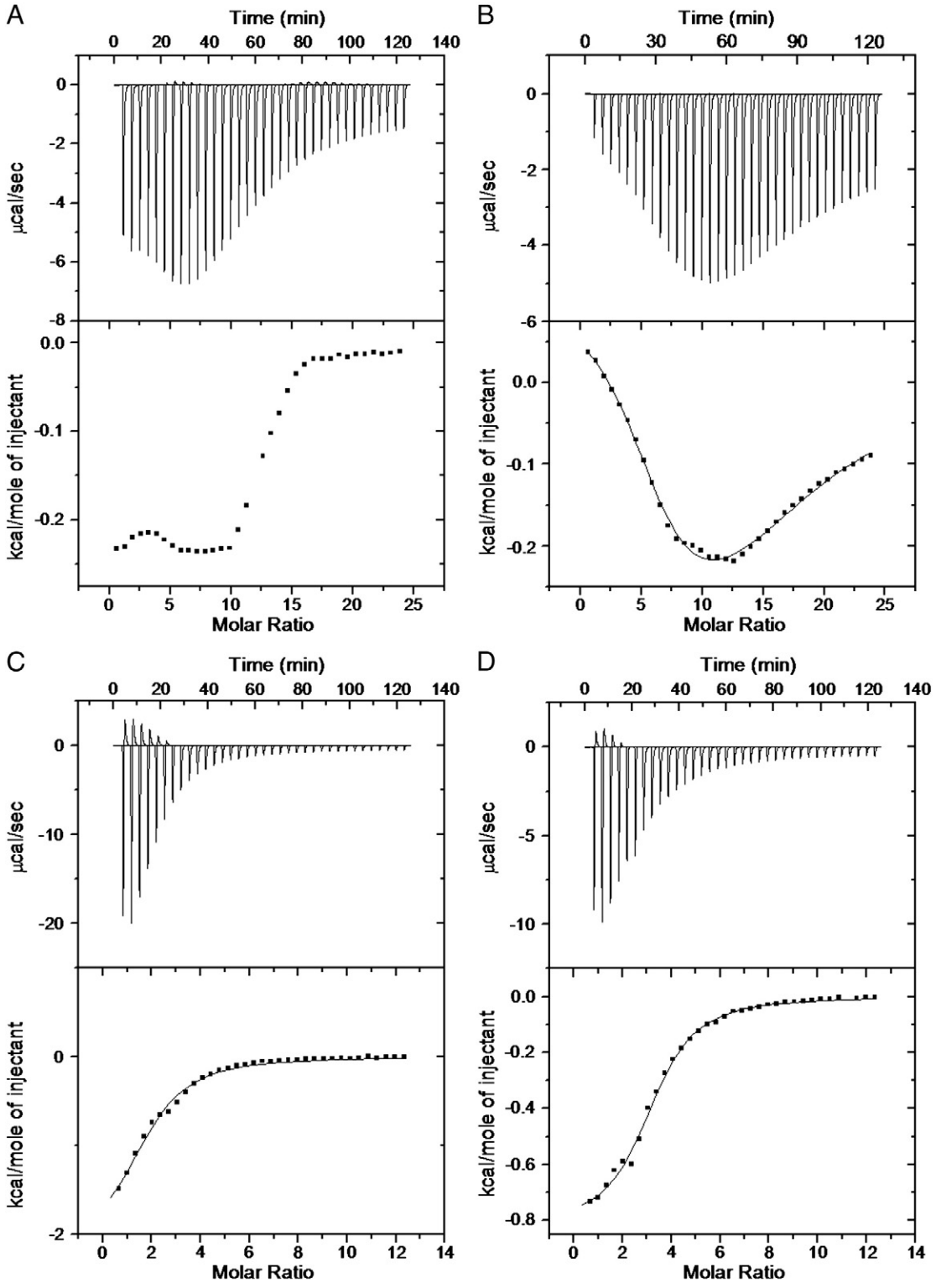

Fig. 4. Calorimetric titration of peptide 1 and 2 with 100 mM $CaCl_2$ or 50 mM $MgCl_2$. The ligand (15 µl injections) was added to the peptide solution at 200 s intervals. A, peptide 1/Ca^{2+}. B, peptide 2/Ca^{2+}. C, peptide 1/Mg^{2+}. D, peptide 2/Mg^{2+}.

arrangement of Gla residues [14–16]. The con-G/Ca^{2+} and con-T [K7Gla]/Ca^{2+} complexes are dimeric assemblies of highly helical strands, but the driving force directing the self-organization is distinguished from canonical coiled-coils and helical bundles [3,21], insofar as they appear to originate and be maintained by electrostatics rather than hydrophobic effects. These structures are also different from metal ion-induced coiled-coils and helical bundles, in which metal ions stabilize the ordered structures [22–27]. However in these latter cases, hydrophobic interactions remain the predominant driving forces for higher order assembly. In order to confirm the common role of Gla residues in self-assembly, we designed the studies described herein.

From sedimentation equilibrium analyses, we have demonstrated that the designed peptide 1 and 2 with Gla arrangements of i, i + 4, i + 7, i + 11, i + 14 can form helical dimers in the presence of 20 mM Ca^{2+} (Table 1), but not Mg^{2+}. This phenomenon mainly arises from the small

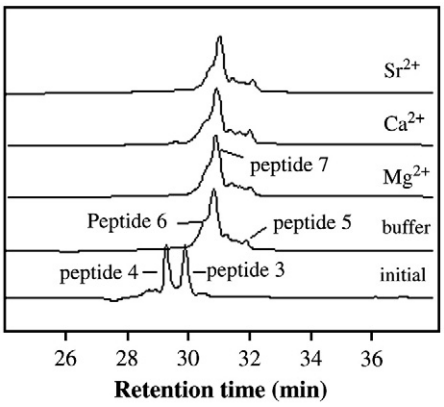

Fig. 5. HPLC analyses of the equilibrium distribution of oxidation products following mixing of peptide 3 and peptide 4 in the presence or absence of various metal ions. The folding buffer was 50 mM $NaBO_3$/100 mM NaCl, pH 8.2. The chloride salts of the indicated divalent metal ions were used at a concentration of 20 mM. The initial concentrations of peptide 3 and peptide 4 were 0.33 mM.

ionic radii of Mg^{2+} and a comparatively high charge-to-radius ratio versus Ca^{2+}. In Gla-containing conantokin peptides, Mg^{2+} displays a high propensity for Gla intrachain, but not interchain binding [28]. On the other hand, Ca^{2+} can accommodate irregular coordination geometries with intrachain and/or interchain Gla residues because of its weak affinity and large ionic radii. Thus, Mg^{2+} shows intrachain interactions with Gla at a lower ratio of Mg^{2+}/peptide (ca., 2–3 mol of Mg^{2+}/mol of monomer, Table 1), whereas Ca^{2+} displays propensities for both intrachain and interchain interactions with Gla residues at a higher ratio of Ca^{2+}/peptide. Such cases were also found in con-G/Ca^{2+} and con-T[K7γ]/Ca^{2+} in which Ca^{2+} assumes mixed intrachain and interchain binding modes [16]. In the case of the disulfide-linked homostranded peptide 5, Ca^{2+} also induces the formation of a helical dimer but not for Mg^{2+}, $Zn^{2+}$and Mn^{2+} (Table 1). Interestingly, the microcalorimetric data have revealed that the two designed peptides have the higher Ca^{2+} binding stoichiometry (more than 6 mol of Ca^{2+}/mol of dimer for first and second binding sites) related to six Gla residues, this is interpreted that some Ca^{2+} chelate to Glu residues. Similarly, Sr^{2+} and Ba^{2+} can form a helical dimer, but Zn^{2+} and Mn^{2+} failed to induce the formation of the helical dimer in these peptides (Table 1).

The observation that the equilibrium distribution of disulfide-bridged peptide 1 does not reflect a strong preference for antiparallel peptide chain orientation suggests that the interface of peptide 1 is significantly different from that found for con-G and con-T[K^7Gla] [14,16]. This is not surprising in light of the results of recent X-ray crystallographic analyses of con-G and con-T[K^7Gla] [16], showing that the differences in some residues results in disparate helix–helix axial alignments. Although these structural differences between con-G and con-T[K^7Gla] do not alter the strand alignment orientation of the dimer, they serve to underscore the contribution that residues outside of the Gla core can make towards the structure of the complex. Numerous examples populate the literature indicating that subtle changes in core (*a* and *d*) or *g* and *e* residues can reverse the orientation and/or alter the stoichiometry of oligomerization [17,29–32].

Overall, the results obtained by extending the Gla network, i, i + 4, i + 7, i + 11, i + 14, within the mimetic peptide scaffold suggests that as more knowledge of the interactions that direct folding in Gla-containing peptides is acquired, Ca^{2+}-mediated Gla interactions can be utilized to obtain dimeric peptides with either parallel or antiparallel chain alignments, as well as inter- or intramolecular helix–helix associations.

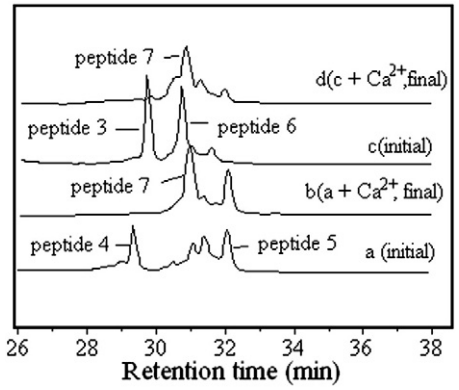

Fig. 6. HPLC-monitored thiol-disulfide exchange assays of peptide 1 variants. The sulfide-linked homodimeric species, peptide 5 and peptide 6, were separately incubated with peptide 4 and peptide 3, respectively. The oxidations were carried out in 50 mM $NaBO_3$/100 mM NaCl, pH 8.2. $CaCl_2$ was present at 20 mM. Chromatograms represent final equilibrium product distributions.

4. Experimental procedures

4.1. Peptide synthesis, purification, and characterization

The methods for synthesis, purification, and characterization of the peptides, as well as the oxidative formation of the disulfide-linked homostranded peptide 5 and peptide 6 and the disulfide-linked heterostranded peptide 7, were similar to those previously described [14].

4.2. Determination of peptide strand orientation

Strand orientation preference was determined using peptide 3 and peptide 4. Typically, a 1:1 molar ratio of peptide 3 and peptide 4 at a concentration of 0.33 mM was stirred in an open vial at room temperature in a total volume of 0.35 mL of folding buffer (50 mM $NaBO_3$/100 mM NaCl, pH 8.2). The progress of the oxidation was monitored by analytical reverse-phase HPLC. Here, 30 μL of the peptide solutions were injected onto an HPLC column (Kromasil C_{18}, 4.6 mm × 250 mm), equilibrated in 90:10 (v:v) 0.1% trifluoroacetic acid (TFA)/$H_2$0:0.1%TFA/CH_3CN at a flow rate of 1.0 mL/min. At a time of 1 min post-injection, a 40 min linear gradient was applied to a limiting value of 55:45(v:v) 0.1% TFA/$H_2$0:0.1%TFA/ CH_3CN. Absorbance detection was performed at 214 nm. Individual peaks were collected, lyophilized and characterized by DE–MALDI–TOF–MS (matrix–assisted delayed extraction laser desorption ionization–time–of–flight mass spectrometry).

The thiol-disulfide rearrangement experiments were carried out under conditions similar to the above folding procedure. The homomeric disulfide-linked peptides, viz., peptide 5 and peptide 6, were dissolved in 50 mM $NaBO_3$/100 mM NaCl, pH 8.2, at concentrations of 330 μM. An aliquot of reduced peptide 3 was added to the peptide 6 solution in a N_2 atmosphere, and an aliquot of reduced peptide 4 was added to the peptide 5 solution, to afford an initial reduced monomer/dimer molar ratio of 2:1. Either $CaCl_2$ or $MgCl_2$ was immediately included to a final concentration of 20 mM. After 1 h, the folding buffer was exposed to air. Aliquots were removed at selected intervals and analyzed by analytical reverse-phase HPLC as described for the oxidation of the reduced peptides.

4.3. CD spectroscopy

CD spectra were recorded between 195 nm and 260 nm on a Jasco J-715 spectropolarimeter using 1 cm pathlength cells. Each spectrum represents the average of three scans collected at a 1.0 nm bandwidth at 1.0 nm intervals. The α-helical content of peptides in solution was determined from the mean residue ellipticities at 222 nm using the empirical relationship, $\text{fraction}_{\text{helix}} = (-[\Theta]_{222} - 2340)/30{,}300$ [33].

4.4. Isothermal titration calorimetry

The binding isotherms of metal ions to the designed peptides were determined at 25 °C on a MicroCal (Northampton, MA) VP-ITC Microcalorimeter in a buffer of 10 mM Na-MES/100 mM NaCl, pH 6.5. Peptide samples ranging in concentration from 0.3–0.5 mM in a total volume of 1.5 ml were introduced into the reaction cell. Injections (3–5 μl) from stock solutions of either 100 mM $CaCl_2$, 50 mM $MgCl_2$, in matching Na-MES buffer, were delivered at discrete intervals. The data were corrected for heats of dilution of the metal ion solution by performing a matching titration of metal ion into buffer in the absence of peptide. The titration curves were deconvoluted for the best-fit model using the ORIGIN for ITC software package supplied by MicroCal.

4.5. Sedimentation equilibrium ultracentrifugation

Sedimentation equilibrium experiments were performed using an Optima XL-I analytical ultracentrifuge (Beckman Instruments, Palo Alto, CA) equipped with a standard two-channel cell in an An-60 Ti rotor. All peptides were dissolved in 10 mM $NaBO_3$/100 mM NaCl buffer, pH 6.5, at a concentration of 150 μM. The peptide samples in the absence of metal ion and in the presence of appropriate concentration of $CaCl_2$, $MgCl_2$, $BaCl_2$, $SrCl_2$, $MnCl_2$, or $ZnCl_2$ were independently rotated at 32,000, 45,000 or 52,000 rpm at 20 °C for 24 h. Absorbance monitoring was performed at 235 nm or 275 nm. The apparent molecular weight (MW_{app}) was obtained by fitting the data to a monomer–dimer equilibrium using the sedimentation analysis software supplied by Beckman. The partial specific volumes used for peptide 1 and peptide 2 were 0.709 and 0.722, respectively, as calculated from the mass average of the partial specific volumes of the individual amino acids [34]. Gla residues were assigned the partial specific volume value of glutamate (0.66 ml/g). The dimer association constants for peptides were calculated by the following equation: $Ka = [dimer]/[monomer]^2$. The concentration of monomer = [starting peptide concentration] × (1 − f_{di}), the concentration of dimer = ([starting peptide concentration] × f_{di})/2, fractional dimer content (f_{di}) was calculated as previously described [14].

Acknowledgements

This work was supported partially by the China Natural Science Foundation (No. 30672446, 90713028), Grant 2006AA09Z404 from the High Technology Program of Oceans in China (to Q.Y.D.), Grant 2010CB529802 from Basic Research Program of China and by grant HL010082 from the National Institutes of Health (to FJC).

References

[1] C. Cohen, D.A. Parry, Science 263 (1994) 488–489.
[2] W.F. DeGrado, C.M. Summa, V. Pavone, F. Nastri, A. Lombardi, Annu. Rev. Biochem. 68 (1999) 779–819.
[3] M.G. Oakley, J.J. Hollenbeck, Curr. Opin. Struct. Biol. 11 (2001) 450–457.
[4] S. Kamtekar, M.H. Hecht, FASEB. J. 9 (1995) 1013–1022.
[5] J.L. Popot, D.M. Engelman, Annu. Rev. Biochem. 69 (2000) 881–922.
[6] S.P. Smith, G.S. Shaw, Biochem. Cell Biol. 76 (1998) 324–333.
[7] L. Regan, Trends Biochem. Sci. 20 (1995) 280–285.
[8] A. Pessi, E. Bianchi, A. Crameri, S. Venturini, A. Tramontano, M. Sollazzo, Nature 362 (1993) 367–369.
[9] M. Matzapetakis, V.L. Pecoraro, J. Am. Chem. Soc. 127 (2005) 18229–18233.
[10] M. Lieberman, T. Sasaki, J. Am. Chem. Soc. 113 (1991) 1470–1471.
[11] T.M. Handel, S.A. Williams, W.F. DeGrado, Science 261 (1993) 879–885.
[12] O.A. Kharenko, M.Y. Ogawa, J. Inorg. Biochem. 98 (2004) 1971–1974.
[13] J. Liu, J. Dai, M. Lu, Biochemistry 42 (2003) 5657–5664.
[14] Q.Y. Dai, M. Prorok, F.J. Castellino, J. Mol. Biol. 336 (2004) 731–744.
[15] Q.Y. Dai, F.J. Castellino, M. Prorok, Biochemistry 43 (2004) 13225–13232.
[16] S.E. Cnudde, M. Prorok, Q.Y. Dai, F.J. Castellino, J.H. Geiger, J. Am. Chem. Soc. 129 (2007) 1586–1593.
[17] O.D. Monera, C.M. Kay, R.S. Hodges, Biochemistry 33 (1994) 3862–3871.
[18] O.D. Monera, N.E. Zhou, C.M. Kay, R.S. Hodges, J. Biol. Chem. 268 (1993) 19218–19227.
[19] P. Burkhard, S. Ivaninskii, A. Lustig, J. Mol. Biol. 318 (2002) 901–910.
[20] R. Fairman, H.G. Chao, T.B. Lavoie, J.J. Villafranca, G.R. Matsueda, J. Novotny, Biochemistry 35 (1996) 2824–2829.
[21] A.N. Lupas, M. Graber, Adv. Protein. Chem. 70 (2005) 37–78.
[22] B.T. Farrer, V.L. Pecoraro, Proc. Natl. Acad. Sci. USA 100 (2003) 3760–3765.
[23] D. Ghosh, V.L. Pecoraro, Inorg. Chem. 43 (2004) 7902–7915.
[24] T. Tanaka, T. Mizuno, S. Fukui, H. Hiroaki, J. Oku, K. Kanaori, K. Tajima, M. Shirakawa, J. Am. Chem. Soc. 126 (2004) 14023–14028.
[25] O. Iranzo, D. Ghosh, V.L. Pecoraro, Inorg. Chem. 45 (2006) 9959–9973.
[26] M. Sirish, S.J. Franklin, J. Inorg. Biochem. 91 (2002) 253–258.
[27] S.N. Dublin, V.P. Conticello, J. Am. Chem. Soc. 130 (2008) 49–51.
[28] S.E. Cnudde, M. Prorok, F.J. Castellino, J.H. Geiger, J. Biol. Inorg. Chem. 15 (2010) 667–675.
[29] M. Oakley, P.S. Kim, Biochemistry 37 (1998) 12603–12610.
[30] O.D. Monera, C.M. Kay, R.S. Hodges, Biochemistry 33 (2001) 3862–3871.
[31] N.A. Schnarr, A.J. Kennan, J. Am. Chem. Soc. 126 (2004) 14447–14451.
[32] C.M. Taylor, A.E. Keating, Biochemistry 44 (2005) 16246–16256.
[33] Y.H. Chen, J.T. Yang, H.M. Martinez, Biochemistry 11 (1972) 4120–4131.
[34] T.M. Laue, B.D. Shah, T.M. Ridgeway, In Analytical Ultracentrifugation in Biochemistry and Polymer Science, The Royal Society of Chemistry, Cambridge, 1992 pp. 90–125.